Novel neuroanatomical integration and scaling define avian brain shape evolution and development.

Akinobu Watanabe[1,2,3,*], Amy M. Balanoff[2,4], Paul M. Gignac[2,5], M. Eugenia Gold[6], Mark A. Norell[2]

Affiliations:

[1]Department of Anatomy, New York Institute of Technology College of Osteopathic Medicine, Old Westbury, NY 11568, USA.

[2]Division of Paleontology, American Museum of Natural History, New York, NY 10024, USA.

[3]Department of Life Sciences Vertebrates Division, Natural History Museum, London, SW7 5BD, UK.

[4]Department of Psychological and Brain Sciences, Johns Hopkins University School of Medicine, Baltimore, MD 21218, USA

[5]Department of Anatomy and Cell Biology, Oklahoma State University Center for Health Sciences, Tulsa, OK 74107, USA.

[6]Biology Department, Suffolk University, Boston, MA 02108, USA.

*For correspondence: Akinobu Watanabe, E-mail: awatanab@nyit.edu

Abstract: How do large and unique brains evolve? Historically, comparative neuroanatomical studies have attributed the evolutionary genesis of highly encephalized brains to deviations along, as well as from, conserved scaling relationships among brain regions. However, the relative contributions of these concerted (integrated) and mosaic (modular) processes as drivers of brain evolution remain unclear, especially in non-mammalian groups. While proportional brain sizes have been the predominant metric used to characterize brain morphology to date, we perform a high-density geometric morphometric analysis on the encephalized brains of crown birds (Neornithes or Aves) compared to their stem taxa—the non-avialan coelurosaurian dinosaurs. When analyzed together with developmental neuroanatomical data of model archosaurs (*Gallus*, *Alligator*), crown birds exhibit a distinct allometric relationship that dictates their brain evolution and development. Furthermore, analyses by neuroanatomical regions reveal that the acquisition of this derived shape-to-size scaling relationship occurred in a mosaic pattern, where the 'avian'-grade optic lobe and cerebellum evolved first among non-avialan dinosaurs, followed by major changes to the evolutionary and developmental dynamics of cerebrum shape after the origin of Avialae. Notably, the brain of crown birds is a more integrated structure than non-avialan archosaurs, implying that diversification of brain morphologies within Neornithes proceeded in a more coordinated manner, perhaps due to spatial constraints and abbreviated growth period. Collectively, these patterns demonstrate a plurality in evolutionary processes that generate encephalized brains in archosaurs and across vertebrates.

Introduction

The human brain, with its inflated cerebrum, is often considered the zenith of brain evolution. Seminal works, both classic and modern, have suggested that our specialized brain morphology arose through (i) changes in gross-level scaling relationship (allometry) of brains (Striedter, 2005; Rilling, 2006;

Passingham and Smaers, 2014), and (ii) mosaic, or modular, evolution where individual brain regions have the capacity to evolve quasi-independently from one another due to decoupling of previously shared genetic, developmental, functional, and spatial constraints (Barton and Harvey, 2000; Rowe et al., 2011; Smaers and Soligo, 2013; Gómez-Robles et al., 2014; Ni et al., 2019). Clarifying the degree to which these patterns extend across vertebrates requires examining other episodes of encephalization. Crown birds offer an excellent comparative system to mammals, even primates, because they share neuroanatomical features that evolved independently, including a relatively large brain size (Jerison, 1973; Nieuwenhuys et al., 1998; Northcutt, 2002; Butler and Hodos, 2005; Iwaniuk et al., 2005; Gill, 2006), globular brains with expanded cerebra, specialized cytoarchitecture and neuron types (Reiner et al., 2004; Dugas-Ford et al., 2012; Shanahan et al., 2013; Pfenning et al., 2014; Karten, 2015; Stacho et al., 2020), and the capacity to perform higher cognitive behaviors (Lefebvre et al., 2002; Weir et al., 2002; Emery, 2006; Auersperg et al., 2012; Kabadayi et al., 2016; von Bayern et al., 2018; Boeckle et al., 2020). In addition, they feature remarkable variation in brain morphology that is conducive to macroevolutionary studies (Iwaniuk and Hurd, 2005) (Figure 1).

Chronicling the evolutionary origins of the archetypal 'avian' brain requires information on ancestral brain morphologies of extinct coelurosaurian dinosaurs. Because brain tissue does not readily fossilize, paleontologists have relied on endocasts, or the internal mold of the braincase, to document and analyze neuroanatomical evolution through geologic time (Jerison, 1963, 1969; Edinger, 1975; Hopson, 1979; Balanoff and Bever, 2017). As in extant mammals, the brain occupies nearly the entire cranial cavity in crown birds, and thus, these endocasts are used as accurate proxies for brain size and shape in these groups (Jerison, 1973; Haight and Nelson, 1987; de Miguel and Henneberg, 1998; Iwaniuk and Nelson, 2002; Watanabe et al., 2019). Volumetric analyses of endocasts from avialan and non-avialan dinosaurs show that crown birds exhibit a derived allometric trend in brain to body size although some closely related non-avialan dinosaurs (e.g., oviraptorosaurs, troodontids) overlap in allometric trends with neornithine groups (Balanoff et al., 2013; Ksepka et al., 2020). Volumetric data of endocasts also indicate that each brain region evolved under different modes across avialan and non-avialan coelurosaurs,

implying mosaic brain evolution (Balanoff et al., 2016b). However, whether the encephalized brains of crown birds possess a truly unique allometric trajectory and a more modular structure than non-avialan archosaurs, as anticipated by classic notion of phenotypic modularity (Wagner and Altenberg, 1996; Goswami et al., 2014), remains to be explicitly tested. In addition, despite its prevalence and importance as a morphological metric, size data are limited in characterizing brain morphology. For example, similarly sized brains could have disparate shapes, especially given the diversity in brain morphologies within Neornithes and similar volumetric proportions between crown birds and some non-avialan dinosaurs.

To holistically analyze neuroanatomical shape, we use a high-density geometric morphometric (GM) approach on endocranial reconstructions from micro-computed tomography (μCT) imaging. Three-dimensional (3-D) landmarks were placed virtually on endocasts from 37 extant and recently extinct (Dodo, Greak Auk) neornithine species and six non-avialan coelurosaurs to characterize the overall morphology of the brain and its functional subdivisions visible on the endocast—cerebrum, optic lobe, cerebellum, and medulla (Figure 1; see Appendix 1—table 1, 2 for specimen and landmark sampling). In this study, endocranial regions are referred to by the name of the soft tissue features that are reflected on the surface. This unified mathematical framework allows the relative size, configuration, and surface morphology of neuroanatomical traits to be analyzed together, including allometric and correlative trends in shape within and between brain regions (Klingenberg, 2008). We analyze this rich phenotypic dataset to test if crown birds exhibit (i) a derived allometric relationship between endocranial shape and size, and (ii) a more structurally modular brain compared to the ancestral pattern observed in non-avialan coelurosaurian dinosaurs. Moreover, we anticipate that differences in evolutionary patterns of allometry and phenotypic integration will be reflected in extant archosaurs developmentally (Bookstein et al., 2003), where clades with more integrated brain evolution show more integrated brain development. As such, we combine postnatal developmental data of the American alligator (*Alligator mississippiensis*) and the domestic chicken (*Gallus gallus*) with interspecific sampling of Coelurosauria to assess whether (iii) the

90 developmental allometry and integration pattern mirror evolutionary patterns of endocranial shapes in
91 non-avialan dinosaurs and crown birds, respectively.
92
93
94 # Results
95
96 Shape data were subjected to principal components (PC) analysis to create morphospaces that visualize
97 patterns of neuroanatomical variation (Figure 2; Figure 2—figure supplement 1 for fully labeled
98 morphospaces). Morphospace of overall endocranial shape shows that Neornithes exhibits distinct brain
99 morphologies from non-avialan archosaurs, i.e., excluding *Archaeopteryx* (multivariate analysis of
100 variance: $R^2 = 0.323$; $P < 0.001$), largely along the PC1 axis (Figure 2a). *Archaeopteryx*, often considered
101 one of the earliest diverging avialan (Pittman et al., 2020), and an unnamed troondontid (IGM 100/1126)
102 occupy an intermediate position between non-avialan dinosaurs and Neornithes, indicating general
103 evolutionary trend towards the neornithine brain form as previously reported (Balanoff et al., 2014;
104 Ksepka et al., 2020). Although size data from endocasts show partial overlap of crown birds and non-
105 avialan coelurosaurs (Balanoff et al., 2013; Ksepka et al., 2020), high-density shape data discriminate
106 these groups more clearly along PC1 axis, which is associated with cerebral expansion, optic lobe
107 position, hindbrain compaction, and brain flexion. Besides the distinction between non-avialan dinosaurs
108 and crown birds, the distribution of endocranial shape variation within Neornithes has a broad, but modest
109 phylogenetic structure with substantial overlap and convergence among subclades (Blomberg's K =
110 0.035; $P = 0.039$; see Appendix 1—table 3 for phylogenetic signal in shape data). The developmental
111 trajectory of *Alligator* occupies the area of morphospace farthest from crown birds, whereas the
112 endocranial shapes of developing *Gallus* lie adjacent to the cluster of crown birds. When morphospaces
113 are constructed for locally aligned shape data of individual brain regions, cerebrum and optic lobe shapes

largely separate *Alligator*, non-avialan coelurosaurs, and crown birds (Figure 2a, b), whereas cerebellum and medulla shapes partially overlap between these major clades (Figure 2c, d).

Upon establishing that non-avialan coelurosaurs and crown birds diverge in overall endocranial shape, we examined whether this difference is associated with deviations in their scaling relationships. After correcting for phylogenetic structure in the data, endocranial size, as measured by log-transformed centroid size, accounts for 24.2% and 4.8% of total endocranial shape variation within non-avialan coelurosaurs and crown birds, respectively (albeit $P > 0.05$; see Appendix 1—table 3 for allometric signal in shape data). Collectively, these values indicate that size captures a relatively small proportion of neuroanatomical variation, especially in crown birds as previously reported (Marugán-Lobón et al., 2016). To visualize how each endocast diverges from the overall allometric trend across all sampled endocasts, we created bivariate plots of PC1 of residuals from the common allometric trend (RSC1) against scores along this allometric trendline (CAC) where increase in its value corresponds to increase in size (Mitteroecker et al., 2004) (Figure 3; Figure 3—figure supplement 2 for fully labeled plots). The plot for overall endocranial shape illustrates that endocranial shape variation of non-avialan dinosaurs and crown birds lies along divergent allometric trajectories (Figure 3a; non-avialan coelurosaur-Neornithes difference in allometric trajectories: $R^2 = 0.273$; $P < 0.001$). Still, a troodontid (IGM 100/1126) and *Archaeopteryx* are positioned between Neornithes and other non-avialan archosaurs in the morphospace of total endocranial shape (Figure 3a). Thus, for their size, the endocranial shapes of these taxa at the nexus of theropod-bird transition exhibit an intermediary form that approaches those of crown birds. When the developmental dataset of *Alligator* and *Gallus* are incorporated into the interspecific data, neuroanatomical changes in developing *Gallus* overlie the interspecific allometric trajectories of crown birds, whereas those in *Alligator* more closely match the interspecific allometric trajectories of non-avialan coelurosaurs (Figure 3a). Multivariate analysis of variance in full shape space rejects the null hypothesis that the allometric trajectories are shared between developing *Alligator* and *Gallus* ($R^2 = 0.609$, $P < 0.001$ respectively). These results clearly indicate that the avian crown possesses a derived brain-to-size relationship that governs their brain shape evolution as well as development.

Next, to investigate whether evolutionary shifts in allometric trajectories occurred in a concerted or mosaic pattern across regions, we compared allometric trajectories for individual brain regions. For all brain regions, endocranial shapes of *Gallus* do not overlap with those of *Alligator* throughout their postnatal development (Figure 3b–e). The degree to which non-avialan coelurosaurs deviate from the allometric trajectories of endocranial shape in *Alligator* and Neornithes varies for each region. In cerebrum shape, the non-avialan coelurosaurs span the intermediate space between *Alligator* and Neornithes (along PC1 residual shape score), with *Archaeopteryx* and the oviraptorid *Citipati* within the cluster of crown birds (Figure 3b). Based on optic lobe shape, non-avialan coelurosaurs are isolated from the allometric trend of *Alligator* but display closer affinity to crown birds and *Archaeopteryx* (Figure 3c). With the cerebellum, the troodontids (*Zanabazar* and IGM 100/1126) follow the allometric trajectory of crown birds, whereas the other non-avialan coelurosaurs align with the developmental trajectory of *Alligator* (Figure 3d). Developmental trajectories of medulla shape are distinct between *Alligator* and *Gallus* but converge as individuals of these taxa grow (Figure 3e). The troodontid (IGM 100/1126) and *Incisivosaurus* exhibit medulla shapes that are more consistent with allometric trends in *Alligator* development, whereas the correspondence of other non-avialan coelurosaurs to the allometric trajectories of medulla shape in *Alligator* or crown birds are ambiguous due to the convergent allometric trajectory at these medulla sizes (Figure 3e).

Lastly, we employed two methods for evaluating the pattern of integration—covariation ratio (CR) (Adams, 2016) and maximum likelihood (ML) (Goswami and Finarelli, 2016) approaches—to calculate and test the strength of correlation between shapes of neuroanatomical regions. Results from these analyses would elucidate whether the derived neornithine allometric trajectory accompanied a shift in the pattern of morphological integration in the brain. We find that non-avialan coelurosaurs and crown birds reveal different patterns of integration (Figure 4; Appendix 1—table 4–6 for within- and between-region correlation values). Both CR and ML analyses indicate that non-avialan coelurosaurs show strong associations between the cerebrum and optic lobe and between the medulla and cerebellum, while only the CR analysis indicates stronger correlation between the cerebrum and medulla. The results for

neornithines show contrasting patterns between analyses, where CR analysis suggests strong integration between the optic lobe and medulla and ML analysis presents a strong correlation between the cerebrum and cerebellum. Despite this discrepancy, comparison of correlation values clearly indicates that integration between brain regions is stronger in crown birds than in non-avialan dinosaurs (Appendix 1—table 4–6). In particular, crown birds possess a cerebellum that is much more strongly integrated with the cerebrum and optic lobe shapes, which are pairs of structures with much weaker correlations in non-avialan dinosaurs.

Developing *Alligator* and *Gallus* also show contrasting patterns of integration. *Alligator* shows the strongest integration between the optic lobe and medulla, with slightly weaker correlation between the cerebrum and optic lobe. In contrast, *Gallus* shows strong integration between the cerebellum and medulla and more moderate correlations between the cerebrum and optic lobe and between the cerebrum and cerebellum. As observed in non-avialan dinosaurs, cerebellum shape in *Alligator* is weakly correlated with cerebrum and optic lobe shapes, whereas these associations are much stronger in developing *Gallus* akin to the evolutionary pattern seen in crown birds. When tested for differences in the effect size of integration, we find that the endocranial shape of crown birds exhibit significantly greater integrated structure than non-avialan dinosaurs ($P < 0.001$ for overall and pairwise regions; Appendix 1—table 7). While statistical significance is lacking for most comparisons in neuroanatomical integration between developing *Alligator* and *Gallus*, the pairwise tests with moderate statistical significance ($P < 0.05$) show that *Gallus* undergoes more integrated shape changes between the cerebrum and cerebellum and between cerebellum and medulla (Appendix 1—table 7).

Discussion

Neornithes Exhibits Derived Brain Shape, Allometry, and Integration Pattern. Our results indicate that crown birds (i) follow a distinct brain shape-to-size scaling relationship and (ii) possess a more integrated brain structure compared to non-avialan archosaurs that (iii) uniquely characterizes their brain development and evolution. While these derived features of a neornithine brain are clearly demonstrated here, the evolutionary origin of these neuroanatomical novelties is complex. First, the proximity of non-avialan coelurosaurs to crown birds in endocranial shape and its allometric trajectory varies across neuroanatomical regions. The shape differences are more pronounced in the cerebrum and optic lobe (Figure 3b, c) than in the hindbrain (Figure 3d, e). *Archaeopteryx* shows closer resemblance to non-avialan coelurosaurs than extant birds in cerebrum, optic lobe, and medulla shapes, demonstrating that the organization of the archetypal 'avian' brain had not emerged by the origin of Avialae, if *Archaeopteryx* is considered one of the earliest diverging avialans (Figure 3b–d). However, allometric trends across regions signify that *Archaeopteryx* possessed an avian-grade shape-to-size relationship for the optic lobe, and nearly so for the cerebrum and cerebellum. In fact, some non-avialan coelurosaurs approach or align with the allometric trends of crown birds, including non-avialan maniraptoran dinosaurs for the optic lobe and troodontids in cerebellum shape. The oviraptorosaur *Citipati* converges on the cerebral shape of *Archaeopteryx* and the extant cormorant *Phalacrocorax* given its size (Figure 3b). These taxon- and region-specific results are consistent with volumetric studies reporting a mosaic assembly of the avian brain form (Balanoff et al., 2016b; Ksepka et al., 2020). Based on our endocranial shape data, we propose that optic lobes approaching 'avian'-grade scaling relationships emerged at least among Pennaraptora; and similarly, 'avian'-grade allometric trend in cerebellum shape first appeared among Paraves prior to the origin of Avialae (possibly convergently). These neuroanatomical innovations were then followed by the acquisition of specialized shape-to-size scaling relationships in the cerebrum along the lineage spanning *Archaeopteryx* to crown birds, potentially coincident with the increased prominence of the Wulst, a dorsal telencephalic eminence that receives somatosensory and visual signals and thought to be involved in information processing and motor control implicated in powered flight (Gold et al., 2016). Notably, this inferred change to cerebrum shape and development is decoupled from cerebrum size

evolution which did not change substantially from non-avialan paravians to crown birds (Balanoff et al., 2013; Ksepka et al., 2020).

A difficulty in pinpointing the evolutionary origin of derived allometric and integration patterns is the dearth of complete endocranial material from early avialan taxa (Walsh and Milner, 2011; Knoll and Kawabe, 2020) and robust developmental series of non-avialan coelurosaurian dinosaurs. This gap in neuroanatomical sampling limits our current ability to precisely determine the timing and tempo of when these neuroanatomical properties evolved. While shape data could not be collected, known braincase and endocast from the purported ornithuran *Cerebavis* from the Cretaceous period features an amalgam of neornithine neuroanatomical features, with globular and laterally expanded cerebra, ventrally positioned optic lobes, anteroposteriorly short and ventrally positioned cerebellum, and strongly flexed profile (although without a well-developed Wulst) (Kurochkin et al., 2007; Walsh and Milner, 2011; Walsh et al., 2016). Based on these observations, the final phases of the acquisition of an avian-grade brain, including the inflated appearance of cerebra, likely occurred along the lineage spanning the divergence of earliest avialans (e.g., *Archaeopteryx*) to the origin of Ornithurae. Future discoveries of exceptionally preserved braincases of Mesozoic stem birds and their inclusion into our endocranial shape data will greatly facilitate our understanding of this key period in amniote brain evolution. Recent discoveries and reconstructions of complete, articulated, and three-dimensionally preserved Mesozoic avialans (Field et al., 2018, 2020) as well as a developmental series of non-avialan dinosaurs (Evans et al., 2009; Lautenschlager and Hübner, 2013; Bullar et al., 2019), provide a promising outlook on comparative studies of brain evolution along the dinosaur-bird transition. Regardless of a punctuated or gradual evolution of avian-grade cerebrum among avialans, our study demonstrates that the brain of the avian crown exhibits a distinct allometric and a more integrated brains as compared to the ancestral, non-avialan archosaurian condition.

Developmental Trends in Coelurosaurian Brain Evolution. Comparative neuroanatomists have long recognized the intimate connection between brain development and evolution. For instance, prolonged

periods of neurogenesis (Allman et al., 1993; Jones and MacLarnon, 2004; Leigh, 2004; Barton and Capellini, 2011; Sayol et al., 2016b; Yu et al., 2018; Gunz et al., 2020) and regions with delayed onset of neurogenesis (Finlay and Darlington, 1995; Finlay et al., 2001; Charvet and Striedter, 2011) have been shown to be associated with greater encephalization across vertebrates. In this study, we analyzed interspecific and developmental data synchronously, allowing inference of evolutionary shifts in developmental sequence and rate of phenotypic changes, termed heterochrony (Gould, 1977; Alberch et al., 1979; McKinney and McNamara, 1991; Klingenberg, 1998). Recently, Beyrand and colleagues proposed that paedomorphosis (retention of ancestrally juvenile brain morphology in adult stages of descendants) through early cessation of development, or progenesis, accounts for the dorsoventrally flexed brain profile in birds relative to non-avialan archosaurs (Beyrand et al., 2019). This mechanistic explanation agrees with the accelerated yet abridged growth period in birds. The same heterochronic process has been invoked for the evolution of the avian skull (Bhullar et al., 2012)—a structure physically, functionally, and developmentally linked to the brain (Young et al., 2010; Gondré-Lewis et al., 2015; Hu et al., 2015).

Surprisingly, we find no evidence of a uniform heterochronic process underlying the evolution of overall endocranial shape from a crocodylian outgroup to crown birds. Both the morphospace and allometric trajectories of endocranial shape visually show that the developmental trajectories of *Alligator* and *Gallus* do not align with the principal evolutionary trajectory from ancestral shapes of non-avialan dinosaurs and crown birds (Figure 2a, 3a). Comparison of these trajectories in full shape space (i.e., without the reduction in dimensionality of the data) further demonstrate that vectors of developmental shape change are different from the vector of ancestral endocranial shapes of coelurosaurs to crown birds ($P < 0.002$). As such, paedomorphosis does not uniformly explain the major brain shape changes that occurred during the theropod-bird transition, given our current sampling. This discordance with the results of previous studies on avian brain and skull evolution may be due to differences in (i) the morphological variation captured by high-density 3-D compared to 2-D data; (ii) the developmental trajectories of brain shape across archosaurs; and (iii) the impact of heterochronic processes across brain

268 regions, where a mixture of forward and backward shifts in developmental processes occurred within
269 localized regions, as has been shown in the cranium (Bhullar et al., 2012; Plateau and Foth, 2020). Of
270 these possibilities, the second hypothesis is especially intriguing because it implies that non-avialan
271 dinosaurs possessed a distinct modality in brain development from crocodylians and crown birds.
272 Histological evidence suggests IGM 100/1126 was an immature individual (Erickson et al., 2007) and its
273 proximity to crown birds in endocast shape may signify that non-avialan dinosaurs had a unique postnatal
274 development that begins with 'avian'-like brain form (extrapolated section of the regression line for non-
275 avialan dinosaurs in Figure 3a).

276 In support of the third possibility above, regional analysis of neuroanatomical shape suggests that
277 differing heterochronic signals within each brain region contribute to the lack of uniform heterochronic
278 signal in our endocast data. Relative to the developmental trend in *Alligator* (decreasing PC1 residual
279 shape scores in Figure 3), the cerebrum, optic lobe, and cerebellum trend towards increasingly
280 paedomorphic shape (greater PC1 residual shape scores) starting from non-avialan dinosaurs and into
281 modern birds (Figure 3b–d). In contrast, crown birds, including hatchling *Gallus*, exhibit derived,
282 relatively more 'mature' medulla shapes beyond those of adult *Alligator*. Taken together, the piecemeal
283 evolutionary assembly of the 'avian' brain may have comprised increasing paedomorphic effect on the
284 cerebrum and optic lobe among non-avialan coelurosaurs and on the cerebellum among paravian
285 dinosaurs, followed by peramorphosis of the medulla at least within crown birds. These mosaic patterns
286 across taxa and anatomical regions only begin to exemplify the complexity of evolutionary and
287 developmental interactions, illustrating how the identification of clear heterochronic signals is often more
288 challenging and nuanced than implied by a single mechanism. As Shea (2002) proclaims regarding
289 human morphology, "there is no central component of heterochronic transformation that predominantly
290 accounts for the bulk of morphogenetic and evolutionary transitions" (p. 95). We observe this pattern for
291 coelurosaurian brain evolution as well.
292

Crown Birds Possess a More Integrated, Not Modular, Brain Structure. Brain evolution has proceeded through a mixture of integrated (concerted) (Finlay and Darlington, 1995; Finlay et al., 2001) and modular (mosaic) (Barton and Harvey, 2000; Hager et al., 2012; Hoops et al., 2017; Sukhum et al., 2018) patterns. Consistent with volumetric studies on avialan and non-avialan coelurosaurian neuroanatomical studies (Iwaniuk et al., 2004; Balanoff et al., 2016b; Sayol et al., 2016a; Moore and DeVoogd, 2017), our study points to both integrated and modular trends shaping their brain evolution via common allometric and regional trends. In humans and chimpanzees, the highly encephalized brain is thought to have coincided with the acquisition of a more modular structure than other mammals (Gómez-Robles et al., 2014). This scenario agrees with the traditional notion that a more modular structure, allowing for quasi-independent changes among regions, promotes the evolution of novel and diverse forms (Wagner, 1996; Wagner and Altenberg, 1996; Klingenberg, 2005). Interestingly, we find that the brains of crown birds are more integrated than those of non-avialan archosaurs, and this difference is broadly reflected, albeit weakly, in the postnatal development of *Gallus* and *Alligator*. This outcome is particularly surprising given that the allometric signal, a strong integrating factor, is greater in non-avialan coelurosaurs than extant birds (Appendix 1—table 3). The avian brain, therefore, counters the notion that structures become increasingly modular through deep time to maintain or increase evolvability (Wagner and Altenberg, 1996). Although seemingly counter-intuitive, recent empirical and simulation studies demonstrate that integrated structures have the capacity to evolve more extreme phenotypes when selection acts along the major axis of variation (Villmoare, 2013; Goswami et al., 2015; Felice et al., 2018; Machado et al., 2018; Rolian, 2019). As such, the neuroanatomical diversity observed across Neornithes could still arise from strongly integrated brain structure. This result aligns with a recent large-scale analysis on volumetric data showing that crown birds possess greater brain-to-body size integration relative to non-avialan dinosaurs (Ksepka et al., 2020). Therefore, a more integrated structure seems to underlie brain shape and size evolution within Neornithes relative to their coelurosaurian ancestors.

Whether the evolution of a highly encephalized brain with inflated cerebrum shape emerged from an ancestrally more modular or the derived, more integrated configuration remains to be examined with

319 additional endocasts from basally divergent members of Avialae. Volumetric evidence indicating pulses
320 of cerebral expansion occurring among non-avialan maniraptoran dinosaurs (Balanoff et al., 2013;
321 Ksepka et al., 2020) suggests that an ancestrally more modular brain allowed for increasingly
322 encephalized brains and globular cerebra to evolve prior to, and perhaps even after, the origin of Avialae.
323 If true, the more integrated brain of crown birds may be a consequence of the subsequent "spatial
324 packing" of brain tissue inside the endocranial cavity, a hypothesis proposed for the flexed profile of
325 some mammalian brains (Lieberman et al., 2008). A more integrated brain could also be attributed to the
326 abbreviated growth period in crown birds which could be reducing the cumulative imprinting of new
327 covariation patterns onto the integration pattern established earlier in development (Hallgrímsson et al.,
328 2009; Goswami et al., 2014).

329 Besides the overall strength of integration, the degree of correlation between regions helps
330 formulate mechanistic explanations based on the premise that strongly integrated regions are thought to
331 emerge through shared spatial, functional, developmental, and genetic factors (Wagner and Altenberg,
332 1996; Klingenberg, 2008; Gómez-Robles et al., 2014). For example, previous studies have shown that the
333 strength of axonal connections in the brain are associated with the extent of cortical surface folds in
334 mammals (Hofman, 2014). Although the link between surface morphology and neuronal connections in
335 avian systems is yet unclear (although see Early *et al.*, 2020), strongly correlated shape changes could
336 also represent functional coordination between regions. Vision is the dominant sensory modality in
337 modern birds (Shimizu et al., 2010; Walsh and Milner, 2011), and their visual pathways include major
338 projections from the optic lobe to the cerebrum, including the Wulst (Wylie et al., 2009; Shimizu et al.,
339 2010). These critical neuronal connections may induce coordinated morphological development and
340 evolution between the cerebrum and optic lobe shapes. Interestingly, non-avialan coelurosaurs exhibit the
341 strongest integration between the cerebrum and optic lobe and within the hindbrain (cerebellum and
342 medulla). The presence of strong integration between the cerebrum and optic lobe in non-avialan
343 coelurosaurs, but not in a developing *Alligator*, is consistent with the inference from allometric
344 trajectories that derived non-avialan coelurosaurs already possessed aspects of the avian-grade cerebrum

and optic lobes. Collectively, these results suggest that key aspects of the 'avian' visual system emerged in non-avialan dinosaurs, preceding the origin of birds and powered flight. Visual acuity, perhaps for predation or signaling through colorful feathers, was likely an important facet of their lifestyle, an evolutionary scenario shared with primate brain evolution (Barton, 1998; Kirk, 2006).

Materials and Methods

Specimens. CT data and endocranial reconstructions were sampled from previously published studies (Balanoff et al., 2013; Gold and Watanabe, 2018; Watanabe et al., 2019). The interspecific dataset includes six non-avialan coelurosaurs, 37 neornithines, and *Archaeopteryx*. Among non-avialan dinosaurs, we sampled coelurosaurs due to their phylogenetic affinity to birds, and crucially, major neuroanatomical regions are visible on their endocasts unlike those of more basally diverging theropods (Paulina-Carabajal et al., 2019). The braincase of *Alioramus* and *Incisivosaurus* are taphonomically deformed which would lead to inaccurate characterization of endocranial shape. Because the endocast of *Alioramus* showed approximately uniform shear, the endocranial model and coordinate data were retrodeformed based on the symmetrization algorithm (Ghosh et al., 2010) implemented in the `Morpho` R package based on discrete landmarks that are bilaterally symmetric (Schlager et al., 2018). In contrast, the endocast of *Incisivosaurus* shows mediolateral compression (Balanoff et al., 2009) which impedes reliable retrodeformation with existing tools. However, *Incisivosaurus* occupies regions of morphospaces that are compatible with other non-avialan coelurosaurs, with the exception of cerebrum shape (Figure 3b). Statistical analyses without *Incisivosaurus* generate results that are consistent with those presented here, including crown birds possessing significantly more integrated brain architecture (PLS effect size difference = 3.911; $P < 0.001$). Therefore, we have presented the results which include endocranial shape data from *Incisivosaurus*.

Rockefeller Wildlife Refuge (Grand Chenier, LA, USA) provided individuals of *Alligator mississippiensis*: five < 1 year old, two 1–2 years old, and two 2–3 years old (n = 11). Older alligator specimens were collected by a nuisance trapper (Vaughan Gators, Tallahassee, FL, USA). Charles River Laboratory (North Franklin, CT, USA) supplied male chicken specimens (*Gallus gallus*) at 1 day, 1 week, 3 weeks, 6 weeks, and >8 weeks of age. Two individuals were sampled for each age group, with the exception of four individuals at 1 day and >8 weeks of age (n = 14). We selected *Gallus* as exemplar taxon for crown birds due to the availability of developmental series and their importance as a model system. The alligator and chicken specimens were submerged in 10% neutral-buffered formalin immediately following euthanasia (Stony Brook IACUC Protocol #236370-1, Oklahoma State University Center for Health Sciences IACUC Protocol #2015-1). These specimens were fixed in 10% neutral-buffered formalin for over 8 weeks before imaging to mitigate distortion in brain morphology (Weisbecker, 2012). Please refer to Watanabe *et al.* (2019) for additional details on sampling and imaging of *Alligator* and *Gallus* specimens.

Imaging & Endocranial Reconstructions. The heads of specimens were CT scanned at multiple institutions using variable scan parameter values to optimize the contrast and resolution of the X-ray images, while also considering available scan time. For larger specimens requiring multiple scans, separate image stacks were fused using the "3D Stitching" function in ImageJ (FIJI) v1.49u (Schindelin et al., 2012). In VGStudio MAX v2.2 (Volume Graphics, Heidelberg, Germany), full image stacks of each specimen were imported, and virtual segmentation was conducted following the protocol outlined by Balanoff and colleagues (2016). Reconstructed endocasts were then exported as 3-D polygon mesh files. Based on the same landmark scheme analyzed in this study, endocasts are known to accurately represent the variation in brain size and shape in archosaurs and follow the same ontogenetic trends as brain shape in *Alligator* and *Gallus* (Watanabe et al., 2019). As such, we considered the directionality and the variance-covariance structure of brain shape to be closely reflected by endocranial shape data given the large-scale comparative sampling of our study.

Morphometric Data. We employed a high-density 3-D landmark-based geometric morphometric approach to characterize the shape and size of endocasts and their major functional regions (Figure 1; Appendix 1—table 2). The landmark scheme combines discrete landmarks with semi-landmarks on curves and surfaces using Landmark Editor v3.6 (Wiley et al., 2005). Its "patch" tool allows the placement of discrete, consistently defined landmarks at junction points of major brain regions (i.e., left and right cerebral hemispheres, optic tecta, cerebellum, medulla) and specified density of semi-landmarks within these partitions (see Supplementary Table S2). Despite its critical role in the neurosensory repertoire, we did not characterize the shape of the olfactory tract and bulbs due to the incomplete preservation of this region in fossil taxa. To extract shape data, we subjected the coordinate data to a generalized Procrustes alignment (Gower, 1975; Rohlf and Slice, 1990) minimizing total bending energy, while allowing semi-landmarks to slide on the mesh surface (Gunz et al., 2005; Gunz and Mitteroecker, 2013). This was achieved using the `slider3d` and `gpagen` functions in the R packages `Morpho` v2.7 (Schlager, 2017) and `geomorph` v3.2.1 (Adams and Otárola-Castillo, 2013), respectively. To remove redundant shape information but also avoid artifacts from aligning one side of bilaterally symmetric structures (Cardini, 2016, 2017), right landmarks were removed after aligning bilateral coordinate data (Bardua et al., 2019). Ultimately, the left and midline landmarks were analyzed, including the left cerebrum (54 landmarks), left optic lobe (29 landmarks), left side of cerebellum (18 landmarks), and left side of medulla (18 landmarks).

We generated two versions of the regional shape datasets—one based on global alignment of entire endocranial data, and second based on local alignment of regional shape data. The former captures variation in both regional shape and relative position within the endocast, whereas the latter dataset exclusively characterizes the intrinsic shape of each region. We primarily report results based on locally aligned regional shape data to mitigate the effect of relative positions of each region on the coordinate data which would inflate the magnitude of integration between regions, as well as shape differences (e.g., optic lobe located posterior to the cerebrum in *Alligator* and posteroventral to the cerebrum in crown

421 birds). Results based on globally aligned regional shape data, along with locally aligned data, are
422 presented in the supplementary information (Appendix 1—table 3, 5, 6; Figure 4—figure supplement 3).
423 Besides shape, log-transformed centroid size of endocasts was calculated from the coordinate data, which
424 are known to be a reliable proxy for brain and body size across birds and alligators (Marugán-Lobón et
425 al., 2016; Watanabe et al., 2019). We assessed the relative magnitude of digitization error by repeatedly
426 collecting landmark data from a 1-day-old chicken (10 replications), which accounted for 2.41% of the
427 total shape variation of the dataset and was thus considered to be negligible.
428
429 **Time-Calibrated Phylogeny.** First, we created a maximum clade credibility tree of extant birds from
430 3000 posterior trees based on Hackett tree backbone available on birdtree.org (Jetz et al., 2012) using
431 `TreeAnnotator` v1.8.1 (Drummond et al., 2012). *Apteryx* sp., *Diomede* sp., and *Eudyptes* sp. in our
432 sampling were treated as *A. australis*, *D. exulans*, and *E. chrysocome* for the purpose of constructing a
433 tree including all sampled taxa in this study. Then, we incorporated *Alligator*, *Archaeopteryx*, and non-
434 avialan dinosaurs to the tree based on the mean age of first occurrence age listed in the Paleobiology
435 Database (paleobiodb.org). Ages of internal nodes were determined by the maximum age between sister
436 groups to which the species belong (e.g., age of Paraves determined by maximum age of
437 Deinonychosauria and Avialae). When the maximum age of sampled specimen was identical to that of its
438 clade, the age of the internal node was set to equally bisect the parent and descendent branch (Bell and
439 Lloyd, 2015). The Dodo (*Raphus cucullatus*) was placed based on estimated divergence from *Caloenas*
440 lineage at 15.1 Ma (Pereira et al., 2007). Similarly, the Great Auk (*Pinguinus impennis*) was placed based
441 on the mean stratigraphic age of earliest occurrence of its sister group *Alca* (Smith, 2015). This combined
442 paleontological and neontological tree was then modified to reflect the updated topology and branch
443 lengths proposed by a recent genomic study (Prum et al., 2015). For sampled species not included in the
444 genomic tree, a closest relative was chosen based on the global tree of birds (Jetz et al., 2012).
445

Analysis. All statistical analyses were performed in R version 3.6.2 (R Core Development Team, 2017). To visualize patterns of neuroanatomical variation, morphospaces for endocasts and their regions (cerebrum, optic lobe, cerebellum, medulla) were constructed using scores from principal components analysis (PCA) on shape data. The degree of phylogenetic signal, allometry, and evolutionary allometry was assessed with the `physignal`, `procD.lm`, and `procD.pgls` functions, respectively, in the `geomorph` package with 1,000 pseudo-replications. These multivariate statistical tests have been demonstrated to be robust against type I error and loss of power associated with specimen and landmark sampling (Adams, 2014a, 2014b; Collyer et al., 2015). For visualizing allometric trends, we plotted the PC1 of residuals from the overall shape to size relationship against scores along this allometric relationship (Mitteroecker et al., 2004). The `CAC` function in the `Morpho` package was used to extract common allometric component scores and residuals from this trend. Statistical differences between endocranial shapes and allometric trajectories between clades were tested with the `procD.lm` function. We used the `angleTest` function in the `Morpho` R package to test for differences between vectors of evolutionary and developmental shape change in full shape space. The evolutionary shape vector was created from ancestral shape reconstruction for Coelurosauria and Neornithes using the `anc.recon` function in the `Rphylopars` package (Goolsby, 2016). Developmental shape vectors were formulated using smallest and largest endocasts sampled for *Alligator* and *Gallus*. Finally, we used two different statistics to measure the degree of integration among the brain regions—rho based on maximum likelihood (Goswami and Finarelli, 2016) and covariance ratio using the `modularity.test` function (Adams, 2016). Although known to be susceptible to specimen and landmark sampling (Adams and Collyer, 2016), results based on correlation coefficients from partial least squares (R_{PLS}) using `integration.test` are also presented in the supplementary information (Appendix 1—table 4, 5). Tests of neuroanatomical integration on crown birds excluded *Gallus* to maintain separation from its developmental analysis. To test for one-tailed differences in the degree of integration between clades, we used the `compare.pls` function in the `geomorph` package which is robust to differences in specimen

and landmark sampling (Adams and Collyer, 2016). For statistical tests of interspecific data, we corrected the shape data for phylogenetic structure based on phylogenetic generalized least-squares method with the exception of allometric trajectory comparison between non-avialan dinosaurs and crown birds.

Acknowledgements

We are indebted to Ruth Elsey, Gregory Erickson, David Kay, Broderick Vaughan, and Doug Warner for providing *Alligator* and *Gallus* specimens; Morgan Hill and Henry Towbin for assistance with CT imaging; Isabelle Brenes and Carolynn Merrill for assistance with processing CT data; and William Harcourt-Smith, Emma Sherratt, and Jesus Marugán-Lobón for helpful discussions.

Additional files

Data availability. Aligned bilateral landmark data with size intact are available as supplementary information (Watanabe_etal_eLife_SIData.txt) and on Dryad (doi:10.5061/dryad.qv9s4mwdk). The dataset is organized as a 2-D matrix, where rows are specimens and columns are coordinate values. The specimen sampling comprises six non-avialan coelurosaurian dinosaurs (Specimen 2, 42, 55, 56, 57, 72 in dataset), Archaeopteryx (Specimen 19), and 38 crown birds (Specimen 1, 17, 18, 20–26, 41, 43–54, 58–71), as well as developmental series of *Alligator* (Specimen 3–16) and *Gallus* (Specimen 27–40). Notably, this dataset includes 225 3-D landmarks with slid landmarks that encompass the bilateral form of endocasts with the scale retained so that centroid size could be calculated. To extract left-sided shape data analyzed in this study, the dataset should first be subjected to typical generalized Procrustes alignment minimizing total Procrustes distance without sliding semi-landmarks. After alignment, the left and median (semi-)landmarks should be extracted: Landmark 1–54, 109–137, 168–170, 173–175, 178–

180, 183–185, 188–190, 193–195, 198–200, 203–205, 208–210, 213–215, 218–220, and 222–224. The resulting dataset is ready to be analyzed and partitioned into left cerebrum (landmarks 1–54), left optic lobe (landmarks 55–83), left side of cerebellum (landmarks 84–101), and left side of medulla (102–119).

Appendix 1. Supplementary tables related to this study.

Figure 2—figure supplement 1. Morphospaces constructed from first two principal components of neuroanatomical shape. These plots illustrate the distribution of shape variation in the **a,** overall endocranial shape; **b,** cerebrum; **c,** optic lobe; **d,** cerebellum; and **e,** medulla. Regional shape data are locally aligned.

Figure 3—figure supplement 2. Bivariate plots of PC1 of residuals from the common allometric component (CAC) against scores along CAC. These plots illustrate neuroanatomical deviations from the overall shape-to-size allometric trend in the **a,** overall endocasts; **b,** cerebrum; **c,** optic lobe; **d,** cerebellum; and **e,** medulla. For each subregion, the locally aligned shape and regional centroid size were used.

Figure 4—figure supplement 3. Pattern of correlation across globally aligned neuroanatomical shapes. a, network diagrams based on between-region covariation ratios (CR) (Adams, 2016). **b,** network diagrams based on correlation coefficient, rho, from maximum likelihood analysis (Goswami and Finarelli, 2016), where the size of the circles represent the degree of within-region correlation. In both sets of diagrams, the thickness of the line segments between regions indicates relative strength of the correlation. Note that the line thickness is based on values within each analysis (i.e., not comparable between diagrams), where the cut-off point is the mean correlation value. Abbreviations: Cl, cerebellum; Cr, cerebrum; Ol, optic lobe; Me, medulla.

References

Adams, D. C. 2014a. A generalized K statistic for estimating phylogenetic signal from shape and other high-dimensional multivariate data. Systematic Biology 63:685–697.

Adams, D. C. 2014b. A method for assessing phylogenetic least squares models for shape and other high-dimensional multivariate data. Evolution 68:2675–2688.

Adams, D. C. 2016. Evaluating modularity in morphometric data: Challenges with the RV coefficient and a new test measure. Methods in Ecology and Evolution 7:565–572.

Adams, D. C., and E. Otárola-Castillo. 2013. geomorph: An R package for the collection and analysis of geometric morphometric shape data. Methods in Ecology and Evolution 4:393–399.

Adams, D. C., and M. L. Collyer. 2016. On the comparison of the strength of morphological integration across morphometric datasets. Evolution 70:2623–2631.

Alberch, P., S. J. Gould, G. F. Oster, and D. B. Wake. 1979. Size and shape in ontogeny and phylogeny. Paleobiology 5:296–317.

Allman, J. M., T. McLaughlin, and A. Hakeem. 1993. Brain structures and life-span in primate species. Proceedings of the National Academy of Sciences of the United States of America 90:3559–3563.

Auersperg, A. M. I., B. Szabo, A. M. P. Von Bayern, and A. Kacelnik. 2012. Spontaneous innovation in tool manufacture and use in a Goffin's cockatoo. Current Biology 22:R903–R904.

Balanoff, A. M., G. S. Bever, M. W. Colbert, J. A. Clarke, D. J. Field, P. M. Gignac, D. T. Ksepka, R. Ridgely, N. A. Smith, C. R. Torres, and L. M. Witmer. 2016a. Best practices for digitally constructing endocranial casts: examples from birds and their dinosaurian relatives. Journal of Anatomy 229:173–190.

543 Balanoff, A. M., and G. S. Bever. 2017. The role of endocasts in the study of brain evolution; pp. 223–
544 241 in J. Kaas (ed.), Evolution of Nervous Systems, 2nd ed. vol. 1. Elsevier, Oxford.

545 Balanoff, A. M., G. S. Bever, and M. A. Norell. 2014. Reconsidering the avian nature of the
546 oviraptorosaur brain (Dinosauria: Theropoda). PLoS ONE 9:1–15.

547 Balanoff, A. M., J. B. Smaers, and A. H. Turner. 2016b. Brain modularity across the theropod-bird
548 transition: testing the influence of flight on neuroanatomical variation. Journal of Anatomy
549 229:204–214.

550 Balanoff, A. M., X. Xu, Y. Kobayashi, and M. A. Norell. 2009. Cranial osteology of the theropod
551 dinosaur *Incisivosaurus gauthieri* (Theropoda: Oviraptorosauria). American Museum Novitates 1–
552 35.

553 Balanoff, A. M., G. S. Bever, T. B. Rowe, and M. A. Norell. 2013. Evolutionary origins of the avian
554 brain. Nature 501:93–96.

555 Bardua, C., R. N. Felice, A. Watanabe, A.-C. Fabre, and A. Goswami. 2019. A practical guide to sliding
556 and surface semilandmarks in morphometric analyses. Integrative Organismal Biology 1:obz016.

557 Barton, R. A. 1998. Visual specialization and brain evolution in primates. Proceedings of the Royal
558 Society B: Biological Sciences 265:1933–1937.

559 Barton, R. A., and P. H. Harvey. 2000. Mosaic evolution of brain structure in mammals. Nature
560 405:1055–1058.

561 Barton, R. A., and I. Capellini. 2011. Maternal investment, life histories, and the costs of brain growth in
562 mammals. Proceedings of the National Academy of Sciences of the United States of America
563 108:6169–6174.

564 von Bayern, A. M. P., S. Danel, A. M. I. Auersperg, B. Mioduszewska, and A. Kacelnik. 2018.
565 Compound tool construction by New Caledonian crows. Scientific Reports 8:15676.

566 Bell, M. A., and G. T. Lloyd. 2015. Strap: An R package for plotting phylogenies against stratigraphy and
567 assessing their stratigraphic congruence. Palaeontology 58:379–389.

568 Beyrand, V., D. F. A. E. Voeten, S. Bureš, V. Fernandez, J. Janáček, D. Jirák, O. Rauhut, and P.
569 Tafforeau. 2019. Multiphase progenetic development shaped the brain of flying archosaurs.
570 Scientific Reports 9:1–15.

571 Bhullar, B.-A. S., J. Marugán-Lobón, F. Racimo, G. S. Bever, T. B. Rowe, M. a Norell, and A.
572 Abzhanov. 2012. Birds have paedomorphic dinosaur skulls. Nature 487:223–226.

573 Boeckle, M., M. Schiestl, A. Frohnwieser, R. Gruber, R. Miller, T. Suddendorf, R. D. Gray, A. H. Taylor,
574 and N. S. Clayton. 2020. New Caledonian crows plan for specific future tool use. Proceedings of
575 Royal Society of Biology 287:20201490.

576 Bookstein, F. L., P. Gunz, P. Mitteroecker, H. Prossinger, K. Schæfer, and H. Seidler. 2003. Cranial
577 integration in *Homo*: singular warps analysis of the midsagittal plane in ontogeny and evolution.
578 Journal of Human Evolution 44:167–187.

579 Bullar, C. M., Q. Zhao, M. J. Benton, and M. J. Ryan. 2019. Ontogenetic braincase development in
580 *Psittacosaurus lujiatunensis* (Dinosauria: Ceratopsia) using micro-computed tomography. PeerJ
581 2019:1–51.

582 Butler, A. B., and W. Hodos. 2005. Comparative Vertebrate Neuroanatomy: Evolution and Adaptation.
583 Wiley-Interscience, pp.

584 Cardini, A. 2016. Lost in the other half: improving accuracy in geometric morphometric analyses of one
585 side of bilaterally symmetric structures. Systematic Biology 65:1096–1106.

586 Cardini, A. 2017. Left, right or both? Estimating and improving accuracy of one-side-only geometric
587 morphometric analyses of cranial variation. Journal of Zoological Systematics and Evolutionary
588 Research 55:1–10.

589 Charvet, C. J., and G. F. Striedter. 2011. Developmental modes and developmental mechanisms can
590 channel brain evolution. Frontiers in Neuroanatomy 5:1–5.

591 Collyer, M. L., D. J. Sekora, and D. C. Adams. 2015. A method for analysis of phenotypic change for
592 phenotypes described by high-dimensional data. Heredity 115:357–365.

593 Drummond, A. J., M. A. Suchard, D. Xie, and A. Rambaut. 2012. Bayesian phylogenetics with BEAUti
594 and the BEAST 1.7. Molecular Biology and Evolution 29:1969–1973.

595 Dugas-Ford, J., J. J. Rowell, and C. W. Ragsdale. 2012. Cell-type homologies and the origins of the
596 neocortex. Proceedings of the National Academy of Sciences 109:16974–9.

597 Early, C. M., A. N. Iwaniuk, R. C. Ridgely, and L. M. Witmer. 2020. Endocast structures are reliable
598 proxies for the sizes of corresponding regions of the brain in extant birds. Journal of Anatomy 1–15.

599 Edinger, T. 1975. Paleoneurology, 1804–1966: an annotated bibliography. Advances in Anatomy,
600 Embryology and Cell Biology 49:12–258.

601 Emery, N. J. 2006. Cognitive ornithology: the evolution of avian intelligence. Philosophical Transactions
602 of the Royal Society B: Biological Sciences 361:23–43.

603 Erickson, G. M., K. Curry Rogers, D. J. Varricchio, M. A. Norell, and X. Xu. 2007. Growth patterns in
604 brooding dinosaurs reveals the timing of sexual maturity in non-avian dinosaurs and genesis of the
605 avian condition. Biology Letters 3:558–561.

606 Evans, D. C., R. Ridgely, and L. M. Witmer. 2009. Endocranial anatomy of lambeosaurine hadrosaurids
607 (Dinosauria: Ornithischia): A sensorineural perspective on cranial crest function. Anatomical
608 Record 292:1315–1337.

609 Felice, R. N., M. Randau, and A. Goswami. 2018. A fly in a tube: macroevolutionary expectations for
610 integrated phenotypes. Evolution 72:2580–2594.

611 Field, D. J., J. Benito, A. Chen, J. W. M. Jagt, and D. T. Ksepka. 2020. Late Cretaceous neornithine from

612 Europe illuminates the origins of crown birds. Nature 579:397–401.

613 Field, D. J., M. Hanson, D. Burnham, L. E. Wilson, K. Super, D. Ehret, J. A. Ebersole, and B. A. S.
614 Bhullar. 2018. Complete *Ichthyornis* skull illuminates mosaic assembly of the avian head. Nature
615 557:96–100.

616 Finlay, B. L., and R. B. Darlington. 1995. Linked regularities in the development and evolution of
617 mammalian brains. Science 268:1578–1584.

618 Finlay, B. L., R. B. Darlington, and N. Nicastro. 2001. Developmental structure in brain evolution.
619 Behavioral and Brain Sciences 24:263–278.

620 Ghosh, D., N. Amenta, and M. Kazhdan. 2010. Closed-form blending of local symmetries. Eurographics
621 Symposium on Geometry Processing 29:1681–1688.

622 Gill, F. B. 2006. Ornithology. W. H. Freeman, New York, pp.

623 Gold, M. E. L., and A. Watanabe. 2018. Flightless birds are not neuroanatomical analogs of non-avian
624 dinosaurs. BMC Evolutionary Biology 18:1–11.

625 Gold, M. E. L., D. Schulz, M. Budassi, P. M. Gignac, P. Vaska, and M. A. Norell. 2016. Flying starlings,
626 PET and the evolution of volant dinosaurs. Current Biology 26:R265–R267.

627 Gómez-Robles, A., W. D. Hopkins, and C. C. Sherwood. 2014. Modular structure facilitates mosaic
628 evolution of the brain in chimpanzees and humans. Nature Communications 5:1–9.

629 Gondré-Lewis, M. C., T. Gboluaje, S. N. Reid, S. Lin, P. Wang, W. Green, R. Diogo, M. N. Fidélia-
630 Lambert, and M. M. Herman. 2015. The human brain and face: mechanisms of cranial, neurological
631 and facial development revealed through malformations of holoprosencephaly, cyclopia and
632 aberrations in chromosome 18. Journal of Anatomy 227:255–267.

633 Goolsby, E. W. 2016. Likelihood-based parameter estimation for high-dimensional phylogenetic
634 comparative models: Overcoming the limitations of “distance-based” methods. Systematic Biology

65:852–870.

Goswami, A., and J. A. Finarelli. 2016. EMMLi: A maximum likelihood approach to the analysis of modularity. Evolution; International Journal of Organic Evolution 70:1622–1637.

Goswami, A., J. B. Smaers, C. Soligo, and P. D. Polly. 2014. The macroevolutionary consequences of phenotypic integration: From development to deep time. Philosophical Transactions of the Royal Society of London. Series B, Biological Sciences 369:20130254.

Goswami, A., W. J. Binder, J. Meachen, and F. R. O'Keefe. 2015. The fossil record of phenotypic integration and modularity: a deep-time perspective on developmental and evolutionary dynamics. Proceedings of the National Academy of Sciences 112:4891–4896.

Gould, S. J. 1977. Ontogeny and Phylogeny. Belknap Press of Harvard University Press, Cambridge, MA, pp.

Gower, J. C. 1975. Generalized Procrustes analysis. Psychometrika 40:33–51.

Gunz, P., and P. Mitteroecker. 2013. Semilandmarks: a method for quantifying curves and surfaces. Hystrix 24:103–109.

Gunz, P., P. Mitteroecker, and F. L. Bookstein. 2005. Semilandmarks in three dimensions; pp. 73–98 in D. E. Slice (ed.), Modern Morphometrics in Physical Anthropology. Kluwer Academic/Plenum Publishers, New York.

Gunz, P., S. Neubauer, D. Falk, P. Tafforeau, A. Le Cabec, T. M. Smith, W. H. Kimbel, F. Spoor, and Z. Alemseged. 2020. *Australopithecus afarensis* endocasts suggest ape-like brain organization and prolonged brain growth. Science Advances 6:eaaz4729.

Hager, R., L. Lu, G. D. Rosen, and R. W. Williams. 2012. Genetic architecture supports mosaic brain evolution and independent brain-body size regulation. Nature Communications 3:1–5.

Haight, J. R., and J. E. Nelson. 1987. A brain that doesn't fit its skull: a comparative study of the brain

658 and endocranium of the koala, Phascolarctos cinereus (Marsupialia: Phascolarctidae).; pp. 331–352
659 in M. Archer (ed.), Possums and Opossums: Studies in Evolution. Surrey Beatty & Sons, Exeter.

660 Hallgrímsson, B., H. Jamniczky, N. M. Young, C. Rolian, T. E. Parsons, J. C. Boughner, and R. S.
661 Marcucio. 2009. Deciphering the palimpsest: studying the relationship between morphological
662 integration and phenotypic covariation. Evolutionary Biology 36:355–376.

663 Hofman, M. A. 2014. Evolution of the human brain: When bigger is better. Frontiers in Neuroanatomy
664 8:1–12.

665 Hoops, D., M. Vidal-García, J. F. P. Ullmann, A. L. Janke, T. Stait-Gardner, D. A. Duchêne, W. S. Price,
666 M. J. Whiting, and J. S. Keogh. 2017. Evidence for concerted and mosaic brain evolution in dragon
667 lizards. Brain, Behavior and Evolution 90:211–223.

668 Hopson, J. A. 1979. Paleoneurology; pp. 39–146 in C. Gans, R. G. Northcutt, and P. Ulinsky (eds.),
669 Biology of the Reptilia, vol. 9. Academic Press, London.

670 Hu, D., N. M. Young, Q. Xu, H. Jamniczky, R. M. Green, W. Mio, R. S. Marcucio, and B. Hallgrimsson.
671 2015. Signals from the brain induce variation in avian facial shape. Developmental Dynamics
672 244:1133–1143.

673 Iwaniuk, A. N., and J. E. Nelson. 2002. Can endocranial volume be used as an estimate of brain size in
674 birds? Canadian Journal of Zoology 80:16–23.

675 Iwaniuk, A. N., and P. L. Hurd. 2005. The evolution of cerebrotypes in birds. Brain, Behavior and
676 Evolution 65:215–230.

677 Iwaniuk, A. N., K. M. Dean, and J. E. Nelson. 2004. A mosaic pattern characterizes the evolution of the
678 avian brain. Proceedings. Biological Sciences / The Royal Society 271:S148-151.

679 Iwaniuk, A. N., K. M. Dean, and J. E. Nelson. 2005. Interspecific allometry of the brain and brain regions
680 in parrots (Psittaciformes): comparisons with other birds and primates. Brain, Behavior and

681 Evolution 65:40–59.

682 Jerison, H. J. 1963. Interpreting the evolution of the brain. Human Biology 35:263–291.

683 Jerison, H. J. 1969. Brain Evolution and Dinosaur Brains. The American Naturalist 103:575–588.

684 Jerison, H. J. 1973. Evolution of the Brain and Intelligence. Academic Press, New York, 482 pp.

685 Jetz, W., G. H. Thomas, J. B. Joy, K. Hartmann, and A. O. Mooers. 2012. The global diversity of birds in
686 space and time. Nature 491:444–8.

687 Jones, K. E., and A. M. MacLarnon. 2004. Affording larger brains: testing hypotheses of mammalian
688 brain evolution on bats. The American Naturalist 164.

689 Kabadayi, C., L. A. Taylor, A. M. P. von Bayern, and M. Osvath. 2016. Ravens, New Caledonian crows
690 and jackdaws parallel great apes in motor self-regulation despite smaller brains. Royal Society Open
691 Science 3:160104.

692 Karten, H. J. 2015. Vertebrate brains and evolutionary connectomics: on the origins of the mammalian
693 "neocortex." Philosophical Transactions of the Royal Society B: Biological Sciences 370:20150060.

694 Kirk, E. C. 2006. Visual influences on primate encephalization. Journal of Human Evolution 51:76–90.

695 Klingenberg, C. P. 1998. Heterochrony and allometry: the analysis of evolutionary change in ontogeny.
696 Biological Review 73:79–123.

697 Klingenberg, C. P. 2005. Developmental constraints, modules, and evolvability; pp. 219–247 in B.
698 Hallgrímsson and B. K. Hall (eds.), Variation. Academic Press, Cambridge, MA.

699 Klingenberg, C. P. 2008. Morphological integration and developmental modularity. Annual Review of
700 Ecology, Evolution, and Systematics 39:115–132.

701 Knoll, F., and S. Kawabe. 2020. Avian palaeoneurology: Reflections on the eve of its 200th anniversary.
702 Journal of Anatomy 236:965–979.

703 Ksepka, D. T., A. M. Balanoff, N. A. Smith, G. S. Bever, B.-A. S. Bhullar, E. Bourdon, E. L. Braun, J. G.
704 Burleigh, J. A. Clarke, M. W. Colbert, J. R. Corfield, F. J. Degrange, V. L. De Pietri, C. M. Early,
705 D. J. Field, P. M. Gignac, M. E. L. Gold, R. T. Kimball, S. Kawabe, L. Lefebvre, J. Marugán-
706 Lobón, C. S. Mongle, A. Morhardt, M. A. Norell, R. C. Ridgely, R. S. Rothman, R. P. Scofield, C.
707 P. Tambussi, C. R. Torres, M. van Tuinen, S. A. Walsh, A. Watanabe, L. M. Witmer, A. K. Wright,
708 L. E. Zanno, E. D. Jarvis, and J. B. Smaers. 2020. Tempo and pattern of avian brain size evolution.
709 Current Biology 30:2026–2036.

710 Kurochkin, E. N., G. J. Dyke, S. V Saveliev, E. M. Pervushov, and E. V Popov. 2007. A fossil brain from
711 the Cretaceous of European Russia and avian sensory evolution. Biology Letters 3:309–313.

712 Lautenschlager, S., and T. Hübner. 2013. Ontogenetic trajectories in the ornithischian endocranium.
713 Journal of Evolutionary Biology 26:2044–2050.

714 Lefebvre, L., N. Nicolakakis, and D. Boire. 2002. Tools and brains in birds. Behaviour 139:939–973.

715 Leigh, S. R. 2004. Brain growth, life history, and cognition in primate and human evolution. American
716 Journal of Primatology 62:139–164.

717 Lieberman, D. E., B. Hallgrímsson, W. Liu, T. E. Parsons, and H. A. Jamniczky. 2008. Spatial packing,
718 cranial base angulation, and craniofacial shape variation in the mammalian skull: testing a new
719 model using mice. Journal of Anatomy 212:720–735.

720 Machado, F. A., T. M. G. Zahn, and G. Marroig. 2018. Evolution of morphological integration in the
721 skull of Carnivora (Mammalia): changes in Canidae lead to increased evolutionary potential of
722 facial traits. Evolution 72:1399–1419.

723 Marugán-Lobón, J., A. Watanabe, and S. Kawabe. 2016. Studying avian encephalization with geometric
724 morphometrics. Journal of Anatomy 229:191–203.

725 McKinney, M. L., and K. J. McNamara. 1991. Heterochrony: The Evolution of Ontogeny. Plenum Press,

726 New York, pp.

727 de Miguel, C., and M. Henneberg. 1998. Encephalization of the koala, *Phascolarctos cinereus*. Australian
728 Mammalogy 20:315–320.

729 Mitteroecker, P., P. Gunz, M. Bernhard, K. Schaefer, and F. L. Bookstein. 2004. Comparison of cranial
730 ontogenetic trajectories among great apes and humans. Journal of Human Evolution 46:679–698.

731 Moore, J. M., and T. J. DeVoogd. 2017. Concerted and mosaic evolution of functional modules in
732 songbird brains. Proceedings of the Royal Society B: Biological Sciences 284:20170469.

733 Ni, X., J. J. Flynn, A. R. Wyss, and C. Zhang. 2019. Cranial endocast of a stem platyrrhine primate and
734 ancestral brain conditions in anthropoids. Science Advances 5:eaav7913.

735 Nieuwenhuys, R., J. Donkelaar, and C. Nicholson. 1998. The Central Nervous System of Vertebrates.
736 Springer, New York, pp.

737 Northcutt, R. G. 2002. Understanding vertebrate brain evolution. Integrative and Comparative Biology
738 42:743–756.

739 Passingham, R. E., and J. B. Smaers. 2014. Is the prefrontal cortex especially enlarged in the human
740 brain? Allometric relations and remapping factors. Brain, Behavior and Evolution 84:156–166.

741 Paulina-Carabajal, A., M. D. Ezcurra, and F. E. Novas. 2019. New information on the braincase and
742 endocranial morphology of the Late Triassic neotheropod *Zupaysaurus rougieri* using computed
743 tomography data. Journal of Vertebrate Paleontology 39:e1630421.

744 Pereira, S. L., K. P. Johnson, D. H. Clayton, and A. J. Baker. 2007. Mitochondrial and nuclear DNA
745 sequences support a Cretaceous origin of Columbiformes and a dispersal-driven radiation in the
746 Paleocene. Systematic Biology 56:656–672.

747 Pfenning, A. R., E. Hara, O. Whitney, M. V Rivas, R. Wang, P. L. Roulhac, J. T. Howard, M. Wirthlin, P.
748 V Lovell, G. Ganapathy, J. Mouncastle, M. A. Moseley, J. W. Thompson, E. J. Soderblom, A. Iriki,

749 M. Kato, M. T. P. Gilbert, G. Zhang, T. Bakken, A. Bongaarts, A. Bernard, E. Lein, C. V Mello, A.
750 J. Hartemink, and E. D. Jarvis. 2014. Convergent transcriptional specializations in the brains of
751 humans and song-learning birds. Science 346:1256846.

752 Pittman, M., J. O'Connor, D. J. Field, A. Turner, W. Ma, P. Makovicky, and X. Xu. 2020. Pennaraptoran
753 systematics. Bulletin of the American Museum of Natural History 440:7–36.

754 Plateau, O., and C. Foth. 2020. Birds have peramorphic skulls, too: anatomical network analyses reveal
755 oppositional heterochronies in avian skull evolution. Communications Biology 3:1–12.

756 Prum, R. O., J. S. Berv, A. Dornburg, D. J. Field, J. P. Townsend, E. M. Lemmon, and A. R. Lemmon.
757 2015. A comprehensive phylogeny of birds (Aves) using targeted next-generation DNA sequencing.
758 Nature 526:569–573.

759 R Core Development Team. 2017. R: A language and environment for statistical computing. .

760 Reiner, A., D. J. Perkel, L. L. Bruce, A. B. Butler, A. Csillag, W. Kuenzel, L. Medina, G. Paxinos, T.
761 Shimizu, G. Striedter, M. Wild, G. F. Ball, S. Durand, O. Gütürkün, D. W. Lee, C. V. Mello, A.
762 Powers, S. A. White, G. Hough, L. Kubikova, T. V. Smulders, K. Wada, J. Dugas-Ford, S. Husband,
763 K. Yamamoto, J. Yu, C. Siang, and E. D. Jarvis. 2004. Revised nomenclature for avian
764 telencephalon and some related brainstem nuclei. Journal of Comparative Neurology 473:377–414.

765 Rilling, J. K. 2006. Human and nonhuman primate brains: are they allometrically scaled versions of the
766 same design? Evolutionary Anthropology 15:65–77.

767 Rohlf, F. J., and D. E. Slice. 1990. Extensions of the Procrustes method for the optimal superimposition
768 of landmarks. Systematic Biology 39:40–59.

769 Rolian, C. 2019. Ecomorphological specialization leads to loss of evolvability in primate limbs. Evolution
770 74:702–715.

771 Rowe, T. B., T. E. Macrini, and Z.-X. Luo. 2011. Fossil evidence on origin of the mammalian brain.

772 Science 332:955–957.

773 Sayol, F., L. Lefebvre, and D. Sol. 2016a. Relative brain size and its relation with the associative pallium
774 in birds. Brain, Behavior and Evolution 87:69–77.

775 Sayol, F., J. Maspons, O. Lapiedra, A. N. Iwaniuk, T. Székely, and D. Sol. 2016b. Environmental
776 variation and the evolution of large brains in birds. Nature Communications 7:13971.

777 Schindelin, J., I. Arganda-Carreras, E. Frise, V. Kaynig, M. Longair, T. Pietzsch, S. Preibisch, C. Rueden,
778 S. Saalfeld, B. Schmid, J.-Y. Tinevez, D. J. White, V. Hartenstein, K. Eliceiri, P. Tomancak, and A.
779 Cardona. 2012. Fiji: an open-source platform for biological-image analysis. Nature Methods 9:676–
780 682.

781 Schlager, S. 2017. Morpho and Rvcg - shape analysis in R: R-packages for geometric morphometrics,
782 shape analysis and surface manipulations; pp. 217–256 in G. Zhen, S. Li, and G. Szekely (eds.),
783 Statistical Shape and Deformation Analysis: Methods, Implementation and Applications. Academic
784 Press.

785 Schlager, S., A. Profico, F. Di Vincenzo, and G. Manzi. 2018. Retrodeformation of fossil specimens
786 based on 3D bilateral semi-landmarks: implementation in the R package "Morpho." PLOS ONE
787 13:e0194073.

788 Shanahan, M., V. P. Bingman, T. Shimizu, M. Wild, and O. Güntürkün. 2013. Large-scale network
789 organization in the avian forebrain: a connectivity matrix and theoretical analysis. Frontiers in
790 Computational Neuroscience 7:89.

791 Shea, B. T. 2002. Are some heterochronic transformations likelier than others?; pp. 79–101 in N.
792 Minugh-Purvis and K. J. McNamara (eds.), Human Evolution Through Developmental Change. The
793 Johns Hopkins University Press, Baltimore.

794 Shimizu, T., T. B. Patton, and S. A. Husband. 2010. Avian visual behavior and the organization of the

telencephalon. Brain, Behavior and Evolution 75:204–217.

Smaers, J. B., and C. Soligo. 2013. Brain reorganization, not relative brain size, primarily characterizes anthropoid brain evolution. Proceedings. Biological Sciences / The Royal Society 280:20130269.

Smith, N. A. 2015. Sixteen vetted fossil calibrations for divergence dating of Charadriiformes (Aves, Neognathae). Palaeontologia Electronica 18:1–18.

Stacho, M., C. Herold, N. Rook, H. Wagner, M. Axer, K. Amunts, and O. Güntürkün. 2020. A cortex-like canonical circuit in the avian forebrain. Science (New York, N.Y.) 369.

Striedter, G. F. 2005. Principles of Brain Evolution. Sinauer Associates, Sunderland, MA, pp.

Sukhum, K. V., J. Shen, and B. A. Carlson. 2018. Extreme enlargement of the cerebellum in a clade of teleost fishes that evolved a novel active sensory system. Current Biology 28:3857–3863.

Villmoare, B. 2013. Morphological integration, evolutionary constraints, and extinction: a computer simulation-based study. Evolutionary Biology 40:76–83.

Wagner, G. P. 1996. Homologues, natural kinds and the evolution of modularity. American Zoologist 36:36–43.

Wagner, G. P., and L. Altenberg. 1996. Perspective: complex adaptations and the evolution of evolvability. Evolution 50:967–976.

Walsh, S., and A. Milner. 2011. Evolution of the avian brain and senses.; pp. 282–305 in G. Dyke and G. Kaiser (eds.), Living Dinosaurs: The Evolutionary History of Modern Birds. John Wiley & Sons, Oxford.

Walsh, S. A., A. C. Milner, and E. Bourdon. 2016. A reappraisal of *Cerebavis cenomanica* (Aves, Ornithurae), from Melovatka, Russia. Journal of Anatomy 229:215–227.

Watanabe, A., P. M. Gignac, A. M. Balanoff, T. L. Green, N. J. Kley, and M. A. Norell. 2019. Are endocasts good proxies for brain size and shape in archosaurs throughout ontogeny? Journal of

818 Anatomy 234:291–305.

819 Weir, A. A. S., J. Chappell, and A. Kacelnik. 2002. Shaping of hooks in New Caledonian crows. Science
820 297:981.

821 Weisbecker, V. 2012. Distortion in formalin-fixed brains: using geometric morphometrics to quantify the
822 worst-case scenario in mice. Brain Structure and Function 217:677–685.

823 Wiley, D. F., N. Amenta, D. A. Alcantara, D. Ghosh, Y. J. Kil, E. Delson, W. E. H. Harcourt-smith, F. J.
824 Rohlf, K. St John, B. Hamann, R. Motani, S. Frost, A. L. Rosenberger, L. Tallman, T. Disotell, and
825 R. O'Neill. 2005. Landmark Editor. .

826 Wylie, D. R. W., C. Gutierrez-Ibanez, J. M. P. Pakan, and A. N. Iwaniuk. 2009. The optic tectum of
827 birds: mapping our way to understanding visual processing. Canadian Journal of Experimental
828 Psychology 63:328–338.

829 Young, N. M., H. J. Chong, D. Hu, B. Hallgrímsson, and R. S. Marcucio. 2010. Quantitative analyses link
830 modulation of sonic hedgehog signaling to continuous variation in facial growth and shape.
831 Development (Cambridge, England) 137:3405–3409.

832 Yu, X., M. J. Zhong, D. Y. Li, L. Jin, W. B. Liao, and A. Kotrschal. 2018. Large-brained frogs mature
833 later and live longer. Evolution 72:1174–1183.

834

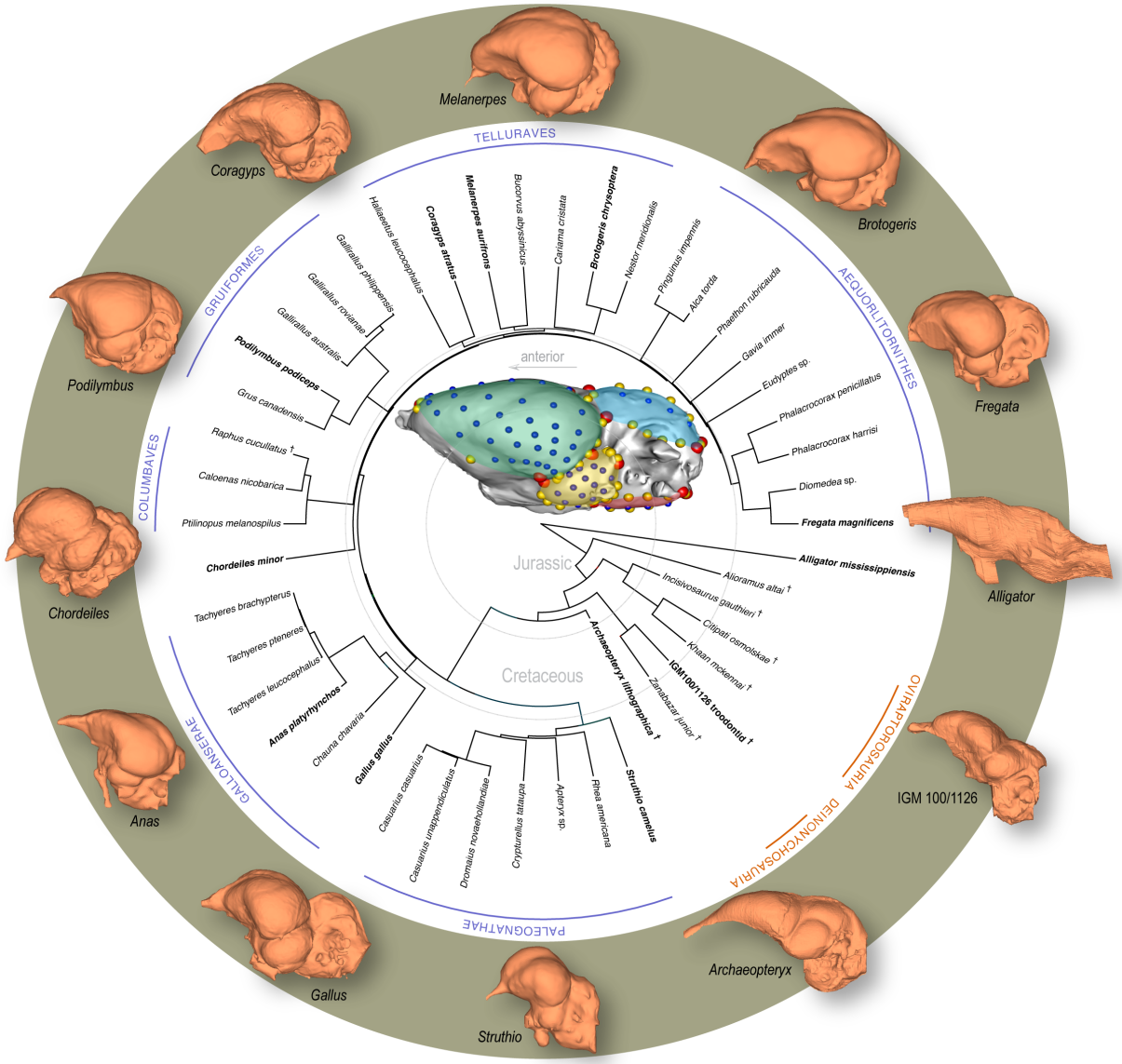

835

836 **Figure 1.** Time-calibrated phylogeny of avialan and non-avialan coelurosaurs sampled in this study, with *Alligator*
837 *mississippiensis* as outgroup. Center image shows discrete (red), curve (yellow), and surface (blue) landmarks used
838 to characterize endocranial shape including the cerebrum (green), optic lobe (yellow), cerebellum (blue), and
839 medulla (red). Lateral views of select endocranial models, indicated by bolded taxonomic names on the phylogeny,
840 highlight the neuroanatomical variation observed across taxa. See Appendix 1—table 1 for list of specimens
841 sampled for the interspecific dataset and Appendix 1-table 2 for the landmark scheme used in this study.

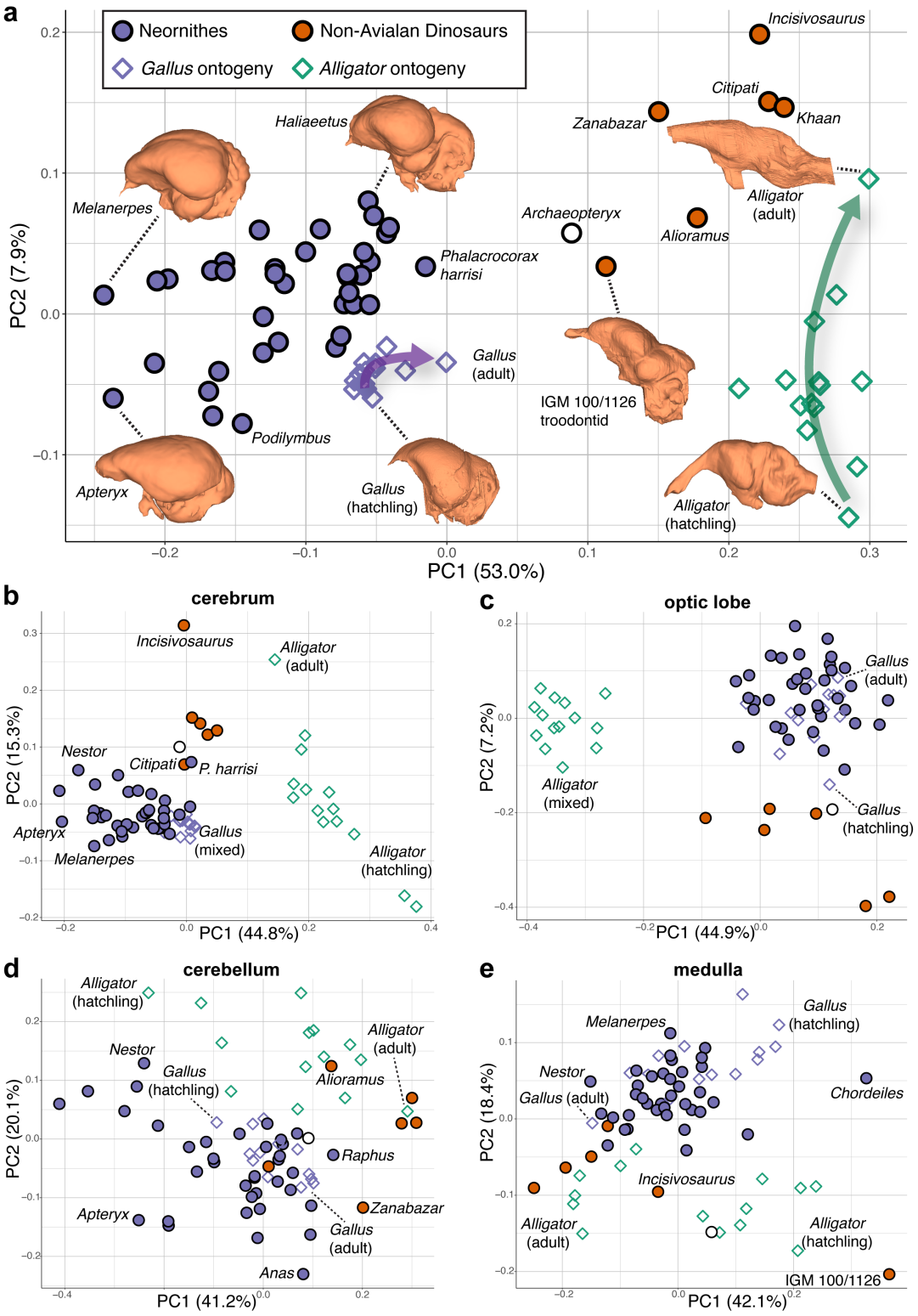

Figure 2. Morphospaces constructed from first two principal components of neuroanatomical shapes. These plots illustrate the distribution of shape variation in the **a,** overall endocranial shape, where the arrows denote postnatal developmental trajectories of *Alligator* (green) and *Gallus* (purple); **b,** cerebrum; **c,** optic lobe; **d,** cerebellum; and **e,** medulla. Regional shape data are locally aligned. See text for details. The following figure supplement is available for figure 2: **Figure supplement 1.** PC morphospaces with full specimen labels.

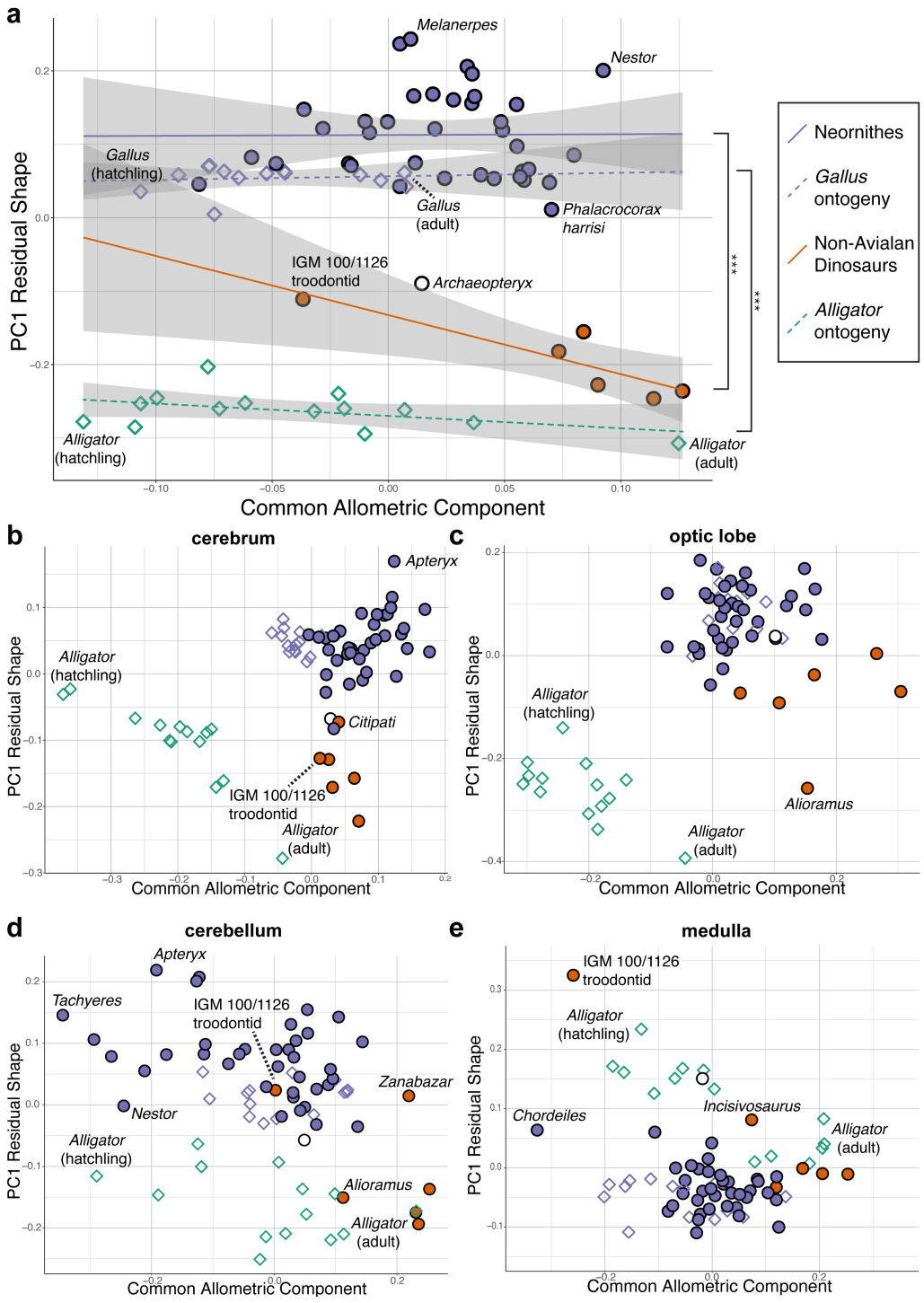

Figure 3. Bivariate plots of PC1 of residuals from the common allometric component (CAC) against scores along CAC (Mitteroecker et al., 2004). These plots illustrate neuroanatomical deviations from the overall shape-to-size allometric trend in the **a,** endocasts (band indicates 95% confidence band), where the null hypothesis that the allometric trajectories between Neornithes and non-avialan dinosaurs and between *Alligator* and *Gallus* are rejected statistically (*** denotes $P < 0.001$); **b,** cerebrum; **c,** optic lobe; **d,** cerebellum; and **e,** medulla. For each subregion, locally aligned shapes and regional log-transformed centroid sizes were used. See text for details. The following figure supplement is available for figure 3: **Figure supplement 2.** PC Plots of PC1 of residuals from CAC against CAC with full specimen labels.

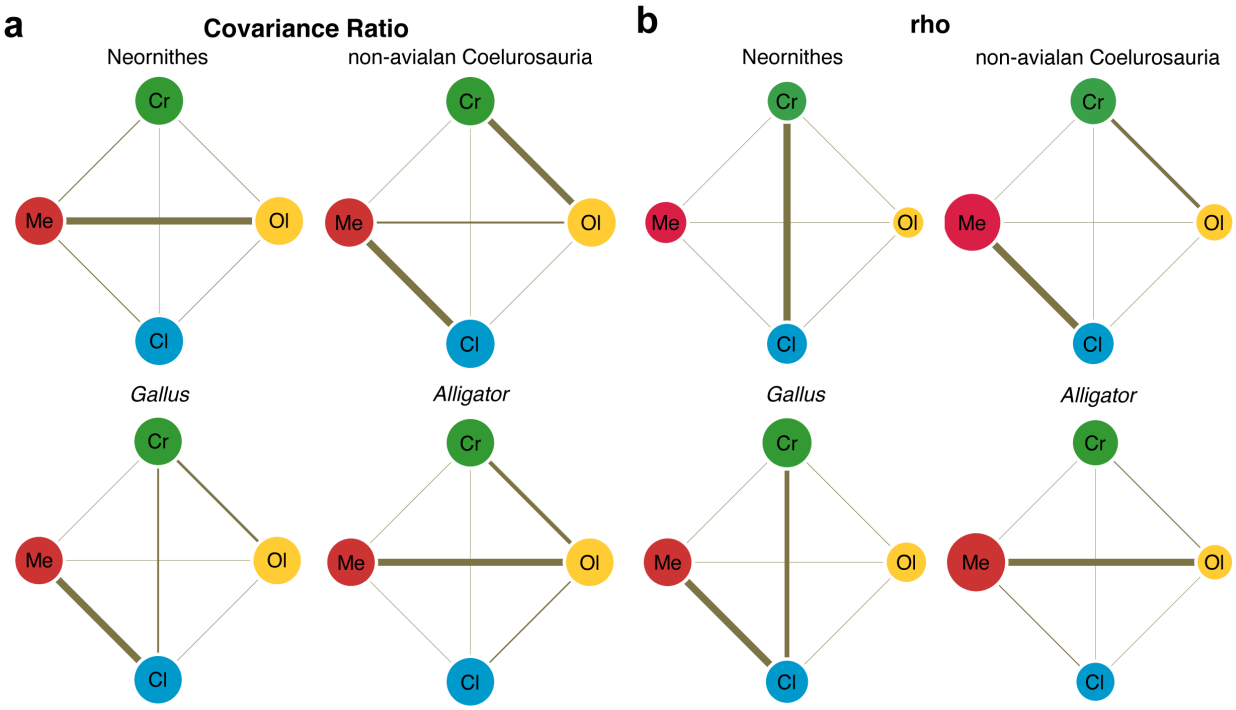

857

858 **Figure 4.** Pattern of correlation across locally aligned neuroanatomical shapes. **a,** network diagrams based on
859 between-region covariance ratios (CR) (Appendix 1—table 4, 6) (Adams, 2016). **b,** network diagrams based on
860 correlation coefficient, rho, from maximum likelihood analysis (Appendix 1—table 4, 6) (Goswami and Finarelli,
861 2016), where the size of the circles represent the degree of within-region correlation. In both sets of diagrams, the
862 thickness of the line segments between regions indicates relative strength of the correlation. Note that the line
863 thickness is based on values within each analysis (i.e., not comparable between diagrams), where the cut-off point is
864 the mean correlation value. Abbreviations: Cl, cerebellum; Cr, cerebrum; Ol, optic lobe; Me, medulla. See text for
865 details. The following figure supplement is available for figure 4: **Figure supplement 3.** Network diagrams of
866 integration within and between globally aligned neuroanatomical regions.

APPENDIX 1

Table 1. List of taxa sampled for this study, with the exclusion of *Alligator* and *Gallus*. Institutional abbreviations: **AMNH,** American Museum of Natural History, New York, NY, USA; **BMNH,** British Museum of Natural History, London, UK; **FMNH,** Field Museum of Natural History, Chicago, IL, USA; **KU,** University of Kansas, Lawrence, KS, USA; **NMNH,** National Museum of Natural History, Washington DC, USA; **TCWC,** Texas Cooperative Wildlife Collection, College Station, TX, USA; **TMM,** Texas Memorial Museum, Austin, TX, USA; **WDC,** Wyoming Dinosaur Center, Thermopolis, WY, USA.

Taxonomic name	Specimen no.
Alioramus altai	IGM 100/1844
Citipati osmolskae	IGM 100/973
Incisivosaurus gauthieri	IVPP V 13326
Unnamed troodontid	IGM 100/1126
Khaan mckennai	IGM 100/973
Zanabazar junior	IGM 100/1
Alca torda	AMNH 17532
Anas platyrhynchos	TMM M-uncat.
Apteryx sp.	TMM M-uncat.
Archaeopteryx lithographica	WDC CSG 100
Brotogeris chrysopteris	FMNH 330249
Bucorvus abyssinicus	TMM M-5946
Caloenas nicobarica	NMNH 19715
Casuarius casuarius	AMNH 3200
Casuarius unappendiculatus	AMNH 2729
Chauna chavaria	KU 81969
Chordeiles minor	TMM M-uncat.
Coragyps atratus	TMM M-uncat.
Crypturellus tataupa	AMNH 8560
Diomedea sp.	TMM M-uncat.
Dromaius novaehollandiae	AMNH 11709
Eudyptes sp.	TMM M-uncat.
Fregata magnificens	FMNH 37858
Gallirallus australis	NMNH 19021
Gallirallus rovianae	AMNH 30329
Gavia immer	TCWC 13.300
Grus canadensis	TMM M-uncat.
Haliaeetus leucocephalus	TMM M-7260
Melanerpes aurifrons	FMNH 108742
Nestor meridionalis	AMNH 27323
Phaethon rubricauda	FMNH 346039
Phalacrocorax harrisi	AMNH 2312
Phalacrocorax penicillatus	TMM M-1180
Pinguinus impennis	AMNH 261
Podilymbus podiceps	TMM M-7139
Ptilinopus melanospila	TMM M-uncat.

Gallirallus philippensis	AMNH 3442
Raphus cucullatus	NHMUK A9040
Rhea americana	AMNH 6470
Cariama cristata	AMNH 8604
Struthio camelus	AMNH 3199
Tachyeres brachypterus	NMNH 555468
Tachyeres leucocephalus	AMNH 8513
Tachyeres pteneres	NMNH 490937

Table 2. List of discrete landmarks and density of semi-landmarks for each neuroanatomical region.

Region	Landmark density	Discrete landmarks
Left/right cerebrum	54	Anterior tip of the cerebrum on dorsal side. Posteromedial point of the left/right cerebrum on dorsal side. Dorsal-most junction point of cerebrum and optic lobe. Ventral-most junction point of cerebrum and optic lobe.
Left/right optic lobe	54	Dorsal-most junction point of cerebrum and optic lobe. Ventral-most junction point of cerebrum and optic lobe. Junction point of optic lobe, midbrain, and medulla. Junction of optic lobe, cerebellum, and medulla.
Cerebellum	30	Anterior-most median point of cerebellum on dorsal side. Left and right anteroventral points of the cerebellum. Left and right dorsal points at the base of flocculus. Left and right posterolateral points of the cerebellum. Posterior-most median point of the cerebellum on dorsal side.
Medulla	29	Anterior-most median point adjacent to midbrain on ventral side. Left and right junctions of optic lobe and medulla. Left and right posterolateral points of medulla. Posterior-most median point of medulla.

Table 3. Phylogenetic signal (Blomberg's *K*), allometry, and evolutionary allometry in endocranial shape. Results generated using `physignal`, `procD.lm`, `procD.pgls` functions in `geomorph` R package v3.2.1 (Adams and Otárola-Castillo, 2013). Results from analysis on globally and locally aligned regions are presented as first and second values within a cell respectively. Allometry evaluated with log-transformed centroid size of the entire endocast and local region respectively. *, **, and *** indicate $P < 0.05$, < 0.01, and <0.001.

Dataset	Region	Phylogenetic signal (*K*)	Allometry (R^2)	Evolutionary allometry (R^2)
Archosauria[1]	overall	0.074***	0.122***	0.039
	cerebrum	0.084*** / 0.044**	0.100* / 0.034	0.034 / 0.371**
	optic lobe	0.082*** / 0.027*	0.135** / 0.054*	0.049 / 0.025
	cerebellum	0.057** / 0.025	0.087* / 0.161**	0.039 / 0.011
	medulla	0.070** / 0.018	0.192*** / 0.242***	0.038 / 0.656***
non-avialan	overall	0.814	0.242	0.242
Coelurosauria	cerebrum	0.761 / 0.680	0.140 / 0.111	0.105 / 0.094
	optic lobe	0.751 / 0.753	0.234 / 0.234	0.224 / 0.195
	cerebellum	0.975* / 0.972*	0.239 / 0.230	0.205 / 0.214
	medulla	0.754 / 0.673	0.375 / 0.680**	0.437* / 0.724**
Neornithes	overall	0.035*	0.093**	0.048
	cerebrum	0.041* / 0.027	0.081* / 0.065*	0.043 / 0.427**
	optic lobe	0.041* / 0.019	0.131*** / 0.034	0.057 / 0.033
	cerebellum	0.033 / 0.021	0.029 / 0.076*	0.046 / 0.016
	medulla	0.023 / 0.015	0.171** / 0.188**	0.051 / 0.720**
Alligator development	overall	—	0.414***	—
	cerebrum	—	0.384*** / 0.356**	—
	optic lobe	—	0.391*** / 0.403***	—
	cerebellum	—	0.375*** / 0.265**	—
	medulla	—	0.523*** / 0.499***	—
Gallus development	overall	—	0.446***	—
	cerebrum	—	0.457*** / 0.399***	—
	optic lobe	—	0.497*** / 0.250***	—
	cerebellum	—	0.329*** / 0.335***	—
	medulla	—	0.472*** / 0.316**	—

[1] excludes developmental series of *Alligator* and *Gallus* but includes their largest specimens.

Table 4. Integration within and between locally aligned neuroanatomical regions. Degree of integration is measured by correlation coefficient from two-block partial least squares analysis (R_{PLS}; upper off-diagonal) and correlation coefficient (ρ; diagonal, lower off-diagonal) using the R packages `geomorph` v3.2.1 (Adams and Otárola-Castillo, 2013) and `EMMLiv2` v0.0.3 (Goswami and Finarelli, 2016) respectively. Interspecific analyses are phylogenetically corrected using phylogenetic generalized least-squares method.

Archosauria

	Cerebrum	Optic Lobe	Cerebellum	Medulla
Cerebrum	0.36	0.991	0.989	0.993
Optic Lobe	0.15	0.31	0.993	0.997
Cerebellum	0.18	0.15	0.36	0.994
Medulla	0.10	0.10	0.11	0.38

non-avialan Coelurosauria

	Cerebrum	Optic Lobe	Cerebellum	Medulla
Cerebrum	0.41	0.989	0.654	0.916
Optic Lobe	0.25	0.33	0.773	0.888
Cerebellum	0.19	0.19	0.37	0.936
Medulla	0.17	0.20	0.29	0.50

Neornithes

	Cerebrum	Optic Lobe	Cerebellum	Medulla
Cerebrum	0.35	0.992	0.990	0.994
Optic Lobe	0.11	0.28	0.993	0.997
Cerebellum	0.15	0.11	0.36	0.994
Medulla	0.10	0.11	0.11	0.37

Alligator development

	Cerebrum	Optic Lobe	Cerebellum	Medulla
Cerebrum	0.41	0.808	0.625	0.688
Optic Lobe	0.20	0.32	0.728	0.913
Cerebellum	0.16	0.16	0.35	0.652
Medulla	0.17	0.27	0.20	0.52

Gallus development

	Cerebrum	Optic Lobe	Cerebellum	Medulla
Cerebrum	0.38	0.966	0.910	0.823
Optic Lobe	0.18	0.31	0.943	0.840
Cerebellum	0.20	0.17	0.33	0.942
Medulla	0.17	0.16	0.21	0.37

Table 5. Integration within and among globally aligned neuroanatomical regions. The degree of integration is measured by correlation coefficient from two-block partial least squares analysis (R_{PLS}; upper off-diagonal) and correlation coefficient (ρ; diagonal, lower off-diagonal) using the R packages `geomorph` v3.2.1 (Adams and Otárola-Castillo, 2013) and `EMMLiv2` v0.0.3 (Goswami and Finarelli, 2016) respectively. Interspecific analyses are phylogenetically corrected using phylogenetic generalized least-squares method.

Archosauria

	Cerebrum	Optic Lobe	Cerebellum	Medulla
Cerebrum	0.43	0.990	0.987	0.991
Optic Lobe	0.28	0.59	0.995	0.995
Cerebellum	0.27	0.35	0.60	0.994
Medulla	0.20	0.29	0.24	0.67

non-avialan Coelurosauria

	Cerebrum	Optic Lobe	Cerebellum	Medulla
Cerebrum	0.46	0.972	0.877	0.867
Optic Lobe	0.36	0.47	0.833	0.808
Cerebellum	0.26	0.30	0.65	0.913
Medulla	0.23	0.35	0.43	0.55

Neornithes

	Cerebrum	Optic Lobe	Cerebellum	Medulla
Cerebrum	0.39	0.991	0.989	0.992
Optic Lobe	0.25	0.47	0.995	0.997
Cerebellum	0.20	0.21	0.49	0.996
Medulla	0.17	0.26	0.22	0.64

Alligator development

	Cerebrum	Optic Lobe	Cerebellum	Medulla
Cerebrum	0.50	0.917	0.927	0.873
Optic Lobe	0.27	0.46	0.911	0.929
Cerebellum	0.29	0.26	0.45	0.866
Medulla	0.15	0.31	0.24	0.51

Gallus development

	Cerebrum	Optic Lobe	Cerebellum	Medulla
Cerebrum	0.43	0.967	0.973	0.824
Optic Lobe	0.31	0.45	0.965	0.893
Cerebellum	0.26	0.28	0.46	0.929
Medulla	0.30	0.38	0.23	0.57

Table 6. Integration between neuroanatomical regions using covariation ratios (CR) (Adams, 2016)**.** Degree of integration between globally aligned regional shapes are listed in the upper off-diagonal elements and that of locally aligned regional shapes in the lower off-diagonal elements. Interspecific analyses are phylogenetically corrected using phylogenetic generalized least-squares method.

Archosauria

	Cerebrum	Optic Lobe	Cerebellum	Medulla
Cerebrum		0.861	0.709	0.944
Optic Lobe	0.899		0.866	0.921
Cerebellum	0.694	0.733		0.758
Medulla	0.883	0.959	0.796	

non-avialan Coelurosauria

	Cerebrum	Optic Lobe	Cerebellum	Medulla
Cerebrum		1.014	0.907	0.823
Optic Lobe	0.991		0.905	0.825
Cerebellum	0.633	0.774		0.949
Medulla	0.739	0.858	1.006	

Neornithes

	Cerebrum	Optic Lobe	Cerebellum	Medulla
Cerebrum		0.877	0.816	0.889
Optic Lobe	0.912		0.951	0.981
Cerebellum	0.797	0.891		0.944
Medulla	0.925	0.998	0.925	

Alligator development

	Cerebrum	Optic Lobe	Cerebellum	Medulla
Cerebrum		0.861	0.877	0.781
Optic Lobe	0.791		0.884	0.920
Cerebellum	0.538	0.696		0.833
Medulla	0.625	0.902	0.581	

Gallus development

	Cerebrum	Optic Lobe	Cerebellum	Medulla
Cerebrum		0.973	0.916	0.792
Optic Lobe	0.908		0.910	0.890
Cerebellum	0.900	0.859		0.865
Medulla	0.781	0.746	0.971	

Table 7. Comparison of integration among neuroanatomical regions using the `compare.pls` function in the `geomorph` R package (Adams and Otárola-Castillo, 2013; Adams and Collyer, 2016). "+" and "–" denote greater and lesser integration in Neornithes and *Gallus* compared to non-avialan coelurosaurs and *Alligator*, respectively. Integration among species calculated upon phylogenetic correction. *, **, and *** indicate $P < 0.05$, < 0.01, and <0.001 (one-tailed). Number preceding and following "/" indicate results based on globally and locally aligned data, respectively.

Neornithes relative to Non-Avialan Coelurosauria (overall: $+^{***}$ / $+^{***}$)

	Cerebrum	Optic Lobe	Cerebellum	Medulla
Cerebrum				
Optic Lobe	$+^{***}$ / $+^{***}$			
Cerebellum	$+^{***}$ / $+^{***}$	$+^{***}$ / $+^{***}$		
Medulla	$+^{***}$ / $+^{***}$	$+^{***}$ / $+^{***}$	$+^{***}$ / $+^{***}$	

Gallus relative to *Alligator* (overall: + / +)

	Cerebrum	Optic Lobe	Cerebellum	Medulla
Cerebrum				
Optic Lobe	+ / +			
Cerebellum	+ / $+^{*}$	+ / +		
Medulla	– / +	– / –	+ / $+^{*}$